JOURNAL OF AIRCRAFT
Vol. 48, No. 2, March–April 2011

Robust Design Optimization of Unmanned Aerial Vehicle Coaxial Rotor Considering Operational Uncertainty

Sangook Jun*
Seoul National University, Seoul 151-744, Republic of Korea
Kwanjung Yee† and Jaewon Lee‡
Pusan National University, Busan 609-735, Republic of Korea
and
Dong-ho Lee§
Seoul National University, Seoul 151-744, Republic of Korea

DOI: 10.2514/1.C001016

This research aims at performing robust design optimization by taking into account operational uncertainties to improve the performance of the coaxial rotor unmanned aerial vehicle that is under development. For this sake, neural network models are constructed for aerodynamic performance obtained from a source-doublet panel method coupled with a time-marching free wake method. Two kinds of operational uncertainties are considered: ballistic damage on blades and weight variation due to the mission change. Approximate moment approach is employed to evaluate the robustness of performance. Subsequently, a relationship between the robustness of performance indices and the parameters representing blade geometry is investigated. In addition, the robustness of the performance indices and constraints for three different solutions chosen from the Pareto optima set is studied. It is confirmed that the trend of design variables to improve performance is in contradiction to the robustness of design. Besides, by incorporating the robust design method, a probability for a designed coaxial rotor to accomplish missions successfully can be improved by 70 ∼ 95% under the uncertainty of ballistic damage.

Nomenclature

C_d, C_D	=	drag coefficient
$C_{d,\text{damage}}$	=	C_d of the damaged airfoil
C_l, C_L	=	lift coefficient
$C_{l\alpha}$	=	C_l at angle of attack zero
$C_{l\alpha,\text{damage}}$	=	$C_{l\alpha}$ of the damaged airfoil
C_P/σ	=	total power coefficient per blade area
C_P	=	total power coefficient
C_T	=	thrust coefficient
C_T/σ	=	thrust coefficient per blade area
D	=	rotor diameter
f	=	objective function
$\bar{f}$	=	averaging objective function
g_i	=	ith constraint
$\bar{g}$	=	averaging constraint
H/D	=	vertical separation between lower and upper rotor
I_R	=	the net inertia of the rotor system
k	=	sigma level
m	=	number of constraints
$\boldsymbol{p}$	=	design parameter vector
$P_{\text{available}}$	=	available power
R_U/R_L	=	differential rotor radii
V_{climb}	=	vertical climb rate
W	=	the weight of the coaxial rotor unmanned aerial vehicle
W_{blade}	=	weight of blades
$\boldsymbol{x}$	=	design variable vector
$\boldsymbol{x^L}$	=	lower bound of design variable vector
$\boldsymbol{x^U}$	=	upper bound of design variable vector
θ	=	pitch angle of blade elements
θ_{75}	=	collective pitch angle
θ_{tw}	=	twist angle
κ	=	induced power factor
Λ	=	anhedral angle
λ	=	inflow rate
σ	=	deviation or solidity
Ω	=	angular velocity
ω	=	weights

Received 10 November 2009; revision received 26 July 2010; accepted for publication 13 November 2010.

*Ph.D., School of Mechanical and Aerospace Engineering, Institute of Advanced Aerospace Technology; ellga5@snu.ac.kr.

†Professor, Department of Aerospace Engineering; daedalus@pusan.ac.kr. Member AIAA.

‡Researcher, Research Institute of Mechanical Technology, San 30 Jangjeon 2-dong Geumjong-gu; andywon@pusan.ac.kr.

§Professor, School of Mechanical and Aerospace Engineering, Institute of Advanced Aerospace Technology; donghlee@snu.ac.kr. Senior Member AIAA.

I. Introduction

INCREASES in crime and budget pressure are forcing the military to seek technologies that allow for a more effective performance of their missions. The concept of having a small and maneuverable unmanned aerial vehicle (UAV) that can be operated in the field to perform sky surveillance, remote sensing, and communication relay is very appealing.

A coaxial rotor configuration can be a viable UAV platform because it provides significant advantages over fixed-wing vehicles by the capabilities of hovering and loitering. Moreover, the coaxial rotor configuration enables a more compact design than the conventional helicopter configuration so that it can be carried by a single person. The small size of the platform also means that it is light weight, thus allowing for easy handling in the field [1].

Mainly inspired by the superior lifting capability and advantages of compact size, Pusan National University started developing a prototype of a small multipurpose UAV [2]. After a series of tradeoff studies in the year 2005, the coaxial rotor system is chosen for the basic platform for the UAV research.

The coaxial rotor UAV is designed for law enforcement purposes, hence it is anticipated to operate in a critical and hazardous environment like in a battle field. As a result, due to unexpected

accidents (operational uncertainty), the rotor performance may be most likely be degraded. The ballistic vulnerability is an important consideration for military helicopters including the coaxial rotor UAV because they generally fly at a lower altitude and slower speed than the fixed-wing aircraft. Therefore, to minimize unexpected attrition of helicopter forces, any performance degradation must be minimized and, if possible, be prevented to ensure a continued success on the battlefield [3]. Since the rotor of helicopters itself provides all forces including lift, propulsion, and control, any damage inflicted to the main rotor systems is more likely to cause serious consequences. In addition, the coaxial rotor UAV is employed in various missions such as reconnaissance, border surveillance, delivery of nonlethal agents, search and rescue support, and chemical/biological agent detection. This means that the UAV carries payloads of diverse types in accordance to the specified flight mission. In certain cases, the payload may exceed the designed total gross weight to enable the mission accomplishment. Since the failure during the given mission may result in the loss of human lives and the valuable vehicle, uncertainty associated with the mission operation is an essential factor to be considered in the design of a coaxial rotor UAV. Consequently, the analysis of robust design optimization is imperative, in the sense that it minimizes the performance degradation by taking into account the operational uncertainty as design requirements.

The robust design optimization is a design method of which the objective is to minimize the deviation of a target performance with respect to an external variation (uncertainty). In a mathematical/statistical sense, one assures robustness by decreasing the size of performance deviation and thus minimizing the performance degradation. To take into account the uncertainty in a system design, one needs to design a system which yields robust performance by incorporating tight tolerance, large safety factor, etc. It follows that experiments are conducted under severe conditions in conjunction with a model in a real scale. This design process repeats until the system satisfies the target performance. However, this method requires enormous cost and time development, while being unable to reduce the performance deviation caused by uncertainty since the optimization requires only minimizing the variations in design variables and the system parameters. Therefore, it is imperative to perform a robust design optimization taking into account the uncertainty given by simple mathematical models.

The history of the robust design optimization ascends to the late 1980s, when Taguchi [4] proposed a methodology of determining design variables that are insensitive to noises in the manufacturing process. His research became the foundation for the robust design, which is followed by intensive researches on the robust design optimization [5–11]. DeLaurentis and Mavris [5] perform a robust design of a high-speed civil transport based on the uncertainty modeling and the formal method for management of uncertainty. Jun et al. [9] use a neural network model in conjunction with Monte–Carlo simulations for the robust design of the wing of an aircraft under the operational and manufacturing uncertainty. Murugan et al. [10,11] discuss the uncertainty analysis of composite material properties for helicopter aeroelastic problems. In light of the remarkable evolution of the robust design optimization, it is meaningful to apply the robust design method to real problems involving actual systems such as a coaxial rotor UAV.

The objective of this research is to design a coaxial rotor UAV that has minimum performance degradation by taking into account the operational uncertainty. To this end, it is important to adopt an aerodynamic analysis method for evaluating performances of a coaxial rotor and a surrogated model that captures the characteristic of performances. For the prediction of aerodynamic performances of a coaxial rotor, Leishman and Ananthan developed the blade element momentum theory (BEMT) for coaxial rotor and solved the local air loads over the upper and lower rotors [1,12,13]. Wachspress and Quackenbush [14] also attempted to enhance the comprehensive hierarchical aeromechanics rotorcraft model (CHARM) comprehensive rotorcraft analysis with a constant vorticity contour (CVC) free wake model to facilitate the aerodynamic and aeroacoustic design of the coaxial rotor systems. Although some previous studies have been proven to be successful and computationally efficient, all of these singularity methods use a vortex lattice representation of the blade and are not capable of predicting the effect of the thickness of the rotor blade. Therefore, this study used a source-doublet panel method with a time-marching free wake model [15,16] for considering the thickness of the rotor because efficiency, accuracy, and robustness are important in the rotor analysis [17,18].

On the other hand, in the conventional design optimization, a second-order polynomial response surface model is often applied as an approximated model for alleviating the burden in the analysis process because a response surface model represents performances as an explicit form of design variables and eliminates some numerical noise [19–21]. However, to evaluate the robustness in a robust design optimization, a surrogated model should be capable of capturing the nonlinearity of performances because a response surface model smoothes a multinodal region and the prediction of a robust region is disturbed. Accordingly, an artificial neural network model is opted as a meta-model in this research for improving the capability of reproducing nonlinear regions in the meta-model of performances [22].

In conjunction with a source-doublet panel method and a neural network, an uncertainty model is built for the ballistic damage and the weight variation due to the mission change. Then an optimization problem is formulated for multiple objectives incorporating different weight parameters between the performance and its variation. In addition, to ensure the robustness of constraints, we add a multiplicative term consisting of the constraints deviation and a sigma level into the constraints. As a consequence, the result of the robust design optimization is compared with that of general design optimization to discuss the importance and the limitation of the robust design optimization. Next, Pareto optimum sets with respect to the sigma level are proposed, and then a relationship between the performance and the robustness is investigated from the tendency of design variables towards robustness. Finally, the performance distribution over the given design region is discussed by observing the Pareto set whenever the sigma level of the constraints increases. The coaxial rotor UAV flies at the advance ratio as low as 0.1, which results in a negligible performance difference between forward-flight and hover. For this reason, the hover performance for the design objective is chosen, from which the performance of the forward-flight of an optimized coaxial rotor UAV is also presented from an off-design analysis.

II. Design Problem Formulation

A. Robust Design Optimization

The conventional design optimization (DO) generally consists of an objective function $f(\boldsymbol{x}, \boldsymbol{p})$ and constraints $g(\boldsymbol{x}, \boldsymbol{p})$, which are given as follows:

$$\begin{aligned} &\text{minimize } f(\boldsymbol{x}, \boldsymbol{p}) \\ &\text{subject to } g_i(\boldsymbol{x}, \boldsymbol{p}) \le 0 \qquad i = 1, \cdots, m \\ &\boldsymbol{x}^L \le \boldsymbol{x} \le \boldsymbol{x}^U \end{aligned} \tag{1}$$

Here, $\boldsymbol{x}$ is the design variable vector and $\boldsymbol{p}$ is the design parameter vector. $\boldsymbol{p}$ is usually regarded as a constant vector in the design process. To transform Eq. (1) into a robust design optimization (RDO) problem involving uncertainty, it is assumed that the design variables and the parameters are independent each other, and they are random variables subject to normal or non-normal distribution. The uncertainties of the design variables and the parameters are related with the objective function and the constraints. Subsequently, the objective functions and constraints end up following arbitrary probability distributions. Therefore, a RDO problem includes deviation σ_f of the objective function and deviation of the constraints σ_g. Then, Eq. (2) is expressed as follows:

$$\begin{aligned} &\text{minimize } \bar{f}(\boldsymbol{x}, \boldsymbol{p}) + \sigma_f \\ &\text{subject to } \bar{g}_i(\boldsymbol{x}, \boldsymbol{p}) + k\sigma_g \le 0 \qquad i = 1, \cdots, m \\ &\boldsymbol{x}^L \le \boldsymbol{x} \le \boldsymbol{x}^U \end{aligned} \tag{2}$$

The sigma level in conjunction with k in the constraints expression is an index that indicates the probability of satisfying the given constraint. For instance, if the sigma level is 2σ, it means that the probability of satisfying the constraint is 95%.

RDO aims at improving performance while ensuring the robustness of the objective function shown in Eq. (2). Thus, as shown in Fig. 1a, the mean value tends to shift representing the performance improvement, while the distribution shrinks representing the robustness which is equivalent to the reduced deviation. On the other hand, the constraints are imposed by a shift as illustrated in Fig. 1b to satisfy a required sigma level because the optimal solution is required to exist in a feasible region (safe region). Figure 2 illustrates the case when one considers these aspects simultaneously. If one considers the robustness of an objective function, as shown in Fig. 2a, the Pareto optima may violate the constraints. However, if the sigma level of constraints has specific values determined by a design requirement or a designer, the confidence interval is completely contained in the safe region as shown in Fig. 2b.

The uncertainty model of the design variables and parameters should be constructed to assess the objective function and constraints in Eq. (2). However, it is nearly impossible to construct the uncertainty model because one lacks the information about when and how the uncertainty will occur. Subsequently, it is reasonable to assume that all uncertainties under consideration follow the normal distribution according to the statement "various natural phenomena follow the Gaussian distribution" [23]. In conjunction with this assumption, the mean and the deviation of the objective function f and the constraints g are determined by using following method to evaluate the robustness. Equation (3) is presented by Taylor series expansion of the objective function and the constraints. The first term means the mean value and the second term is the deviation due to small disturbance of the design variables

$$f(x) = f(\bar{x}) + \sum_{i=1}^{n} \frac{\partial f}{\partial x_i}(x_i - \bar{x}_i)$$

$$g(x) = g(\bar{x}) + \sum_{i=1}^{n} \frac{\partial g}{\partial x_i}(x_i - \bar{x}_i) \tag{3}$$

In this place, as shown in Eq. (4), the mean and the variance are expressed from approximate moment approach (AMA) [8] and the definition of variance

$$\bar{f} = f(\bar{x}), \qquad \sigma_f^2 = \sum_{i=1}^{n} \left(\frac{\partial f}{\partial x_i} \sigma_{xi} \right)^2$$

$$\bar{g} = g(\bar{x}), \qquad \sigma_g^2 = \sum_{i=1}^{n} \left(\frac{\partial g}{\partial x_i} \sigma_{xi} \right)^2 \tag{4}$$

Figure 3 illustrates the design flow of the RDO adopted for this research. The selection of uncertainty parameters and the construction of uncertainty models are added to a DO method. This approach can be told as an augmentation of the robust concept to the DO, where an objective function and constraints are defined by the robustness indices as mentioned earlier.

B. Baseline Configuration

The main mission profile for the coaxial rotor UAV in this research is toward urban intelligence gathering. The overall size of the UAV is restricted to no more than 2 meters in diameter for the sake of compactness and mobility. The takeoff gross weight is chosen as 14 kg including a 4 kg payload, while the flight range and the maximum duration are expected to be 2 km and 30 min, respectively. The UAV should be able to carry extra weight up to 1 kg to accomplish two other selective missions such as delivery of nonlethal agents and chemical biological agent detection. Furthermore, the UAV should retain its performance regardless of a mission failure so that it can be ensured for at least a safe return upon ballistic blade damage on a battlefield. Note that these design requirements are only temporary and could be modified in the development stages by the users or designers.

Figure 4 shows a coaxial UAV prototype developed by the Pusan National University, taking into account the design requirements discussed above, which is based on a series of tradeoff studies and statistical data [15,16,24,25]. This coaxial UAV is adopted for a baseline configuration for the design optimization given in the

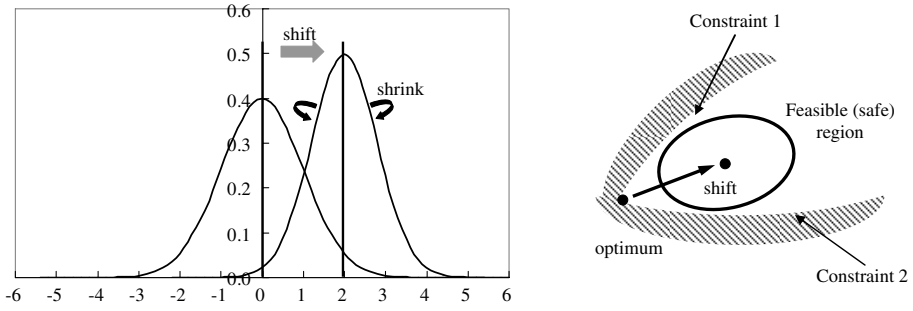

a) Shift and shrink for objective function **b) Shift for constraints**

Fig. 1 Objective function and constraints in robust design optimization.

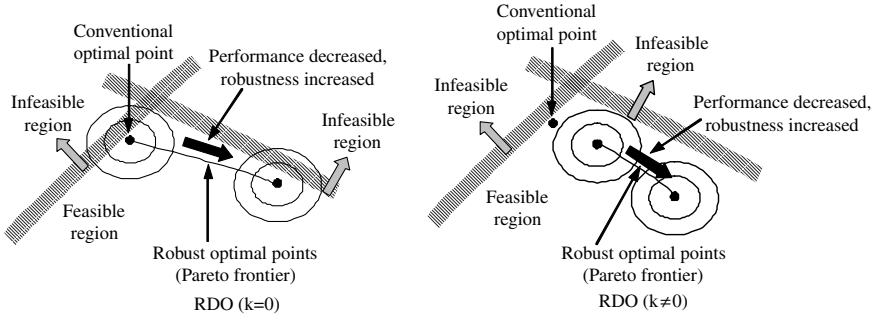

a) Sigma level, k=0 **b) Sigma level ($k \neq 0$)**

Fig. 2 Schematics of Pareto optima in robust design optimization.

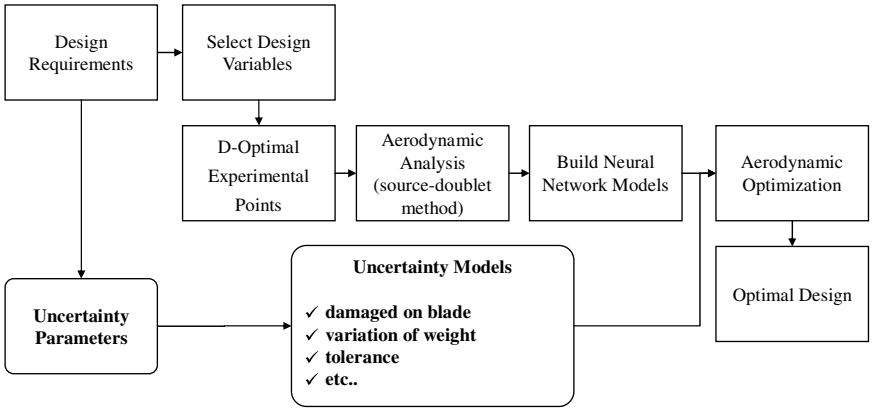

Fig. 3 Procedure of robust design optimization.

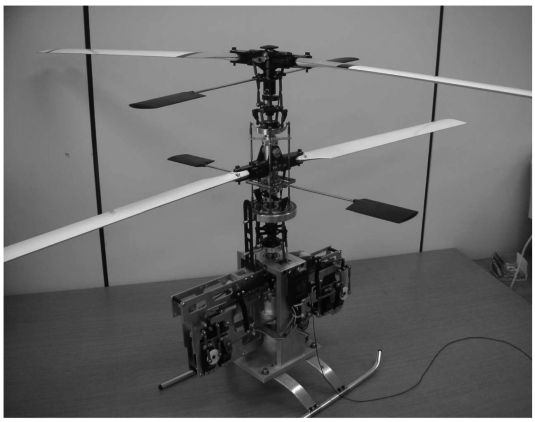

Fig. 4 Configuration of the coaxial rotor UAV designed by the Pusan National University.

following. An electric motor with batteries against an internal engine with fuel is selected for the drive system, which ensures low noise, small vibration, and little detectability.

The rotor geometry and the flight performance of the baseline coaxial rotor are summarized in Table 1. The term vertical separation means that the upper rotor is separated from the lower one by a distance of $0.12D$. The rotor performance in Table 1 is calculated taking the takeoff gross weight of 14 kg and the rotor RPM of 1240 into consideration. The thrust required for hovering is 137.34 N and the figure of merit is about 0.53, which is a little lower as compared with a full-scale conventional helicopter.

Figure 4 shows a coaxial UAV prototype developed by the Pusan National University, taking into account the design requirements discussed above, which is based on a series of tradeoff studies and statistical data. This coaxial UAV is adopted for a baseline configuration for the design optimization given in the following. An electric motor with batteries against an internal engine with fuel is selected for the drive system, which ensures low noise, small vibration, and little detectability.

C. Aerodynamic Analysis

For the design purpose of a coaxial rotor, an efficient aerodynamic analysis tool that provides a faithful outcome like the panel method is necessary. Lee et al. [15,16] developed a source-doublet panel method with a time-marching free wake model to investigate the aerodynamic performance associated with the various configuration parameters. This method takes into account not only the effect of thickness of the rotor blade, but also the complex configurations with varying sectional airfoil, hence providing highly accurate estimates of aerodynamic performance. Consequently, we use the source-doublet panel method with a time-marching free wake model developed by Lee et al. [15,16].

Tip wake geometry in hover and steady forward flight is shown in Fig. 5, in which wake are continuously generated to simulate the temporal evolution of the rotor wake. The solution of the Laplace equation was obtained assuming incompressible and irrotational flow, while considering a local kinematic velocity and the Kutta condition. The wake model is used to simulate the deformation of the wake caused by contraction. The free wake concept allows the vorticity to evolve in a free motion, thus appearing as a physically correct approach to the unsteady aerodynamics. The stability of the rotor wake is an important issue when analyzing hover performance by incorporating the free wake model, and is assured by considering the diffusion of vortex filament core. In addition, because a source-doublet panel code is unable to address the viscous drag, a two-dimensional airfoil table should be incorporated to exactly calculate the profile rotor power. The airfoil table is generally given at a high Reynolds number of orders $10^6 \sim 10^7$. It is necessary to scale the given airfoil table to match with a current Reynolds number because the drag (or the profile rotor power) is sensitive to the Reynolds number. More details about Reynolds number scaling for drag estimation are referred to Wachspress and Quackenbush's research

Table 1 Baseline configuration and performance of the coaxial rotor UAV

Coaxial rotor geometry		Performance	
Rotor diameter (D)	1572 mm	C_T/σ	0.0578
Differential rotor radii (R_U/R_L)	1	C_P/σ	0.0058
Anhedral angle	0.0°	FM	0.5396
Twist	0.0°	GW	14.0 kg
Taper	1	Thrust	137.34 N
Vertical separation (H/D)	0.120	AI	9.2863
Airfoil	VR13	Weight of blade (W_{blade})	0.5520 kg
Solidity (σ)	0.0955	Vertical climb rate (V_{climb})	87.37 m/min
		Available power ($P_{\text{available}}$)	200.0 W

[a]*R_L is $D/2$.

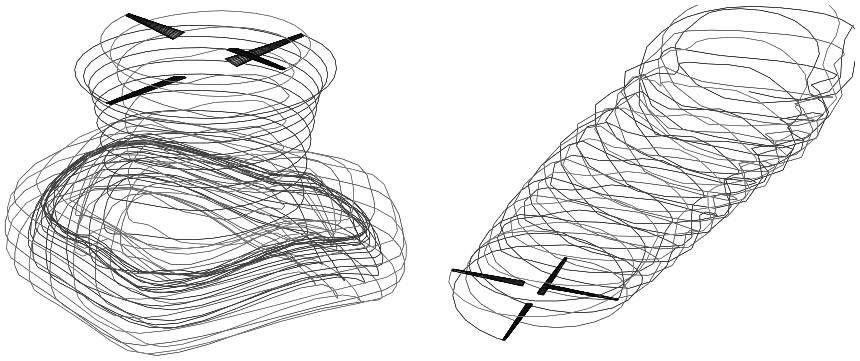

Fig. 5 Hover and steady forward flight results of a source-doublet panel method with a time-marching free wake model.

[14]. Rigorous aerodynamic analysis and the validation can be found in the reference by Lee et al. [15,16].

D. Selection of Design Variables

Table 2 summarizes the range of interest for each design parameter in the parametric study by Lee et al. [15,16], which are based on statistical data and the results of various researches in this field.

Figure 6 shows the relative effects of each design parameter on the rotor performance (the figure of merit and C_P/σ) with a fixed thrust of 137.34 N. The percentage value of each item represents the average variation related to each parameter, which is summed up to 100% across all the parameters varying between the lower and the upper bounds of each parameter. For the airfoil portion, the performance variation is due to change of the airfoil from the NACA0015 to the VR13. This graph shows that the main effect is due to the rotor diameter, whereas the twist and the airfoil effect is relatively small, which differs a little from intuition and physical trends. However, it is enough to find the least effective parameters on the rotor performance, given the range of design parameters in Table 2.

In Fig. 6, the influence of anhedral angle and H/D on two performance indices is less than 3%. Because the anhedral angle is usually used in conjunction with swept back tips, this parameter becomes insignificant for the rectangular type blade of the current study. In addition, the vertical separation between the upper and lower rotors is known to have little effect on the hover performance [14,26]. As a result, the anhedral angle and H/D are excluded from the design variables to be considered.

Among the design parameters, the airfoil shape is a major parameter that has the most significant impact on hover performance. However, the airfoil shape optimization is beyond the scope of this study due to the fact that the shape optimization requires a number of design variables, hence making it inapplicable for practical designs. Based on parametric studies by Lee et al. [15], we choose the VR13 airfoil for this research since it shows superior aerodynamic performance over any other airfoils.

Finally, the rotor diameter, the differential rotor radii (R_U/R_L), the taper, and the twist angle are opted for design variables, of which the upper and lower bounds are chosen according to the ranges in Table 2. Furthermore, the collective pitch angle is incorporated to take into account the rotor trim. The anhedral angle and the vertical separation (H/D) as design parameters are fixed at 0 deg and $0.12D$, respectively.

Table 2 Ranges of design parameters

Design parameters	Lower bound	Upper bound
Rotor diameter ($D = 1572$ mm)	$0.9D$	$1.1D$
Differential rotor radii (R_U/R_L)	0.8	1.0
Anhedral angle	0°	20°
Twist, deg	−14°	−8°
Taper	1	3
Vertical separation (H/D)	$0.108D$	$0.132D$
Airfoil	VR13	

[a]*R_L is $D/2$.

E. Definition of the Uncertainty Model

For the RDO in this study, we construct two uncertainty models in terms of design variables and parameters, namely the operational uncertainty and the manufacturing uncertainty. The operational uncertainty contains ballistic damage of airfoil, deformation of airfoil due to dust, payload change, and varying maximum operational range or endurance time. In this study we are unable to directly incorporate the maximum operational range of the endurance time because of the use of hover performance. Nonetheless, we take these uncertainties into consideration in the manner that the extension of range or endurance time is indirectly related to the weight increase due to the extra battery packs required for the extended operation. In addition, we model the degradation of the rotor performance caused by ballistic damage, dust, or icing, as the reduced lift and drag coefficients as well as the area decrease due to the damaged blade. Furthermore, the manufacturing tolerance is modeled as an uncertainty, albeit it has little effect on the coaxial rotor UAV operation.

1. *Damaged Blade Area*

The variations of C_l, C_d resulting from the damage or deformation of an airfoil are correlated with each other, which implies that it is unlikely to get constant C_d with decreasing C_l. As a matter of fact, finding the relationship between these two variables is difficult, thus we determine the values of C_l, and C_d whose values are rendered maximum by using the results obtained from different research. Then we always incorporate the fixed values of C_l, and C_d to estimate the performance of the rotor blade. With an extra parameter of the area change due to the damaged or deformed blade, we construct an uncertainty model which deals with the performance degradation of the airfoil due to the ballistic damage, dust, or icing.

In accordance with the experimental study on a ballistic damage of the SC1095-R8 Airfoil by Leishman [3,27], a hole close to the leading edge is known to cause the maximum reduction of the aerodynamic performance (40% decrease in C_l, 300% increase in C_d) when the airfoil is subject to the stall angle of attack of 15 deg. The Boeing 737-200 wing model dealing with the effects of ice on lift and drag [28] shows that 30% decrease of C_L and 200% increase of C_D at the stall angle of attack. The NLF0414 airfoil appears to have $30 \sim 40\%$ reduction of C_l due to the effect of the ice over of the stall region [29]. Because the information about the VR13 airfoil in damaged conditions lacks in the literature, we prefer to adopt the results from Leishman (40% decrease in C_l, 300% increase in C_d), albeit being obtained for different airfoil as compared with the VR13. Subsequently, the performance degradation related to the thrust and the required power due to airfoil damages is formulated as a function with respect to the blade area.

It was assumed that the blade tip and the leading edge which are the most critical part from the ballistic damage effect are damaged. Additionally, thrust coefficient C_T and power coefficient C_P of the damaged blade are derived from the equations in [3]. Because the

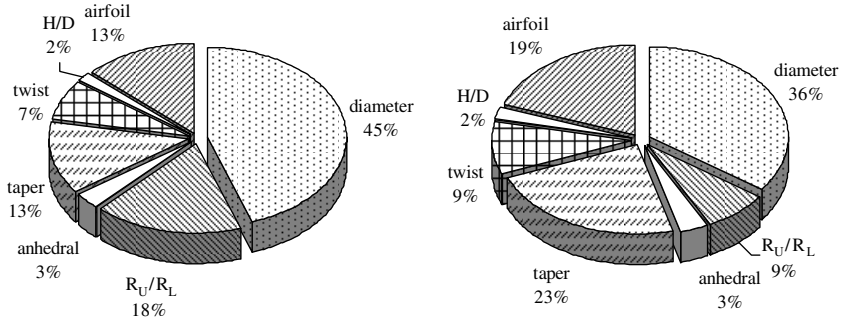

a) C_P/σ **b) Figure of merit**

Fig. 6 Influence of the design parameters on hover performance.

information about SC1095-R8 airfoil is used in damaged conditions, C_T and C_P are the estimated values obtained from Eqs. (5) and (7). It follows that the thrust coefficient C_T can be given in Eq. (5)

$$C_T = \frac{1}{2}\sigma C_{l\alpha}\int_0^d [\theta(r)r^2 - \lambda(r)r]\,\mathrm{d}r + \frac{1}{2}\sigma C_{l\alpha,\mathrm{damage}} \times \int_d^1 [\theta(r)r^2 - \lambda(r)r]\,\mathrm{d}r \quad \text{where,}\ C_{l\alpha,\mathrm{damage}} = 0.6C_{l\alpha} \tag{5}$$

where the integration interval is chosen as [0, 1] which ranges from the root to the tip radius, and d is the starting location of the damage chosen from $0 \le d \le 1$. In addition, the second term $C_{l\alpha,\mathrm{damage}}$ in the right-hand side is the $C_{l\alpha}$ of the damaged airfoil, which is reduced by 40% from the nominal one by taking into account the 40% reduction of C_l.

Because we assume linearly twisted blades in this study, the pitch angle at the blade element $\theta(r)$ can be calculated by using the reference blade-pitch angle (collective pitch, θ_{75}) at the 3/4-radius and the blade twist rate per radius of the rotor (θ_{tw}). In addition, at the hovering condition, the inflow rate $\lambda(r)$ can be expressed in a simple form in Eq. (6)

$$\theta(r) = \theta_{75} + (r - 0.75)\theta_{\mathrm{tw}}$$
$$\lambda(r) = \frac{\sigma C_{l\alpha}}{16}\left(\sqrt{1 + \frac{32}{\sigma C_{l\alpha}}\theta(r)r} - 1\right) \tag{6}$$

From Eqs. (5) and (6), it follows that the C_T is a function of collective pitch angle and damaged area, as shown in Fig. 7.

Figure 7 shows that the C_T is reduced by 9.7 and 17.4% corresponding to 5% damage and 10% damage over no damage at the same collective pitch, respectively. Also, to maintain the hover condition, the collective pitch should be increased, which has an effect on reduced stall margin and therefore a smaller flight envelope.

On the other hand, the total power coefficient C_P is expressed by a sum of the induced power (the first and second terms on the right-hand side) and the profile power (the third and fourth terms on the right-hand side), as given in Eq. (7). Note that $C_{d,\mathrm{damage}}$ represents the C_d of the damaged airfoil, which is 300% greater than nominal one

$$C_P = \int_{r=0}^{r=d}\lambda(r)\,\mathrm{d}C_T + \left[\int_{r=d}^{r=1}\lambda(r)\,\mathrm{d}C_T\right]_{\mathrm{damage}} + \frac{1}{2}\int_0^d \sigma C_d r^3\,\mathrm{d}r + \frac{1}{2}\int_d^1 \sigma C_{d,\mathrm{damage}} r^3\,\mathrm{d}r, \quad \text{where,}\ C_{d,\mathrm{damage}} = 3C_d \tag{7}$$

Finally, along the definition of figure of merit (FM) in Eq. (8), it can be obtained by using Eqs. (5) and (7) as follows:

$$\mathrm{FM} = \frac{\text{ideal power}}{\text{induced power} + \text{profile power}} = \frac{P_{\mathrm{ideal}}}{\kappa P_{\mathrm{ideal}} + P_0} \tag{8}$$

We adopt $\kappa = 1.2$ since we deal with a coaxial rotor UAV as opposed to a conventional helicopter, which has been determined via a graph fitting method using the FM obtained from the approximate model.

Figure 8 illustrates the hover performance via Eqs. (7) and (8), which shows that attaining the same thrust at 10% damage requires 30% increase in the C_P, and the FM decreases by 17% from no damage condition.

The uncertainty model discussed so far is constructed for the case of ballistic damage in the battlefield, however, it can possibly be adopted to deal with the rotor performance variation due to icing or dust by incorporating the blade area change.

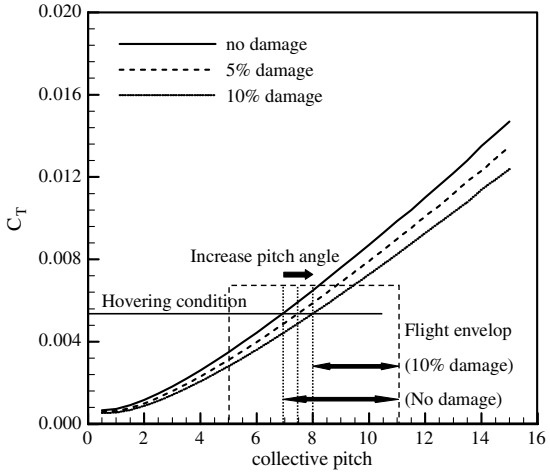

Fig. 7 Variation in rotor thrust coefficient with collective pitch for rotors with different damaged area.

2. Mission Change

To accomplish various missions such as reconnaissance and rescue support, various different types of payload should be considered. For instance, it might be the case that an additional battery pack is needed to improve the endurance time or the operational range, as mentioned earlier. The takeoff gross weight is chosen by 14 kg, however, a multirole coaxial rotor UAV should be designed such that it has the operational performance in spite of the overweight. Hence, we construct an uncertainty model which deals with not only the payload variation due to mission change but also the total weight change of the system.

3. Tolerance

The tolerance uncertainty, albeit nonfatal to the UAV operation, is an uncertainty which often occurs in the manufacturing process. Even though a complete elimination of the tolerance uncertainty seems to be unattainable, most of this uncertainty effect can probably be removed by precision manufacturing at significant cost. In

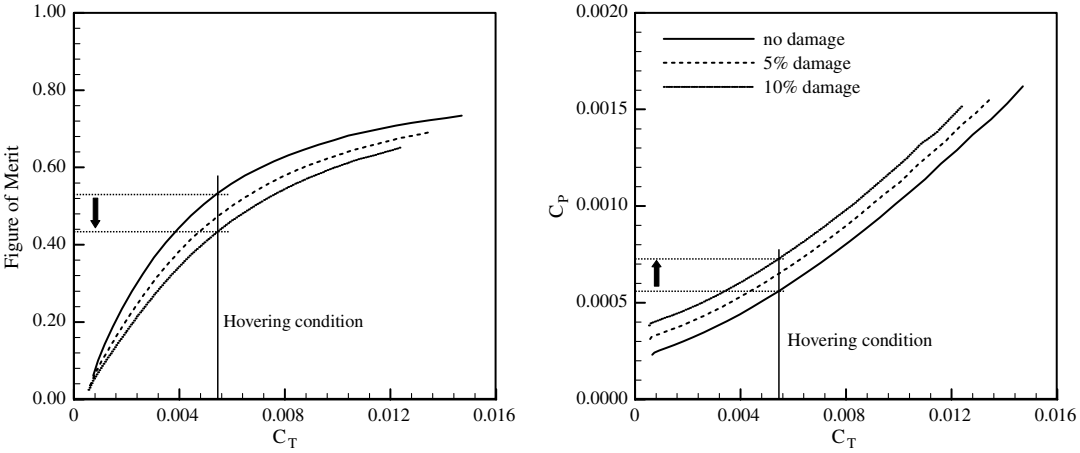

Fig. 8 Hover performance degradation due to ballistic damage on blade.

contrast, by taking into account the tolerance effect on the design stage one can take advantage of not only easy accessibility of fabrication, but also cost reduction. Consequently, in this study we specify the tolerance of the rotor geometry by 2% variation of the design variable ranges in Table 2. The tolerance variation is randomly chosen for the purpose of identifying a major factor affecting the operation of the coaxial rotor UAV such as the operational uncertainty.

Table 3 summarizes the uncertainty models discussed so far, where the deviations of each model are determined based on the design requirements.

Here, A is the total area of four blades and the coefficients with the term VR13 represent the C_l and C_d of the VR13 airfoil. The RDO problem defined in following section is solved by employing the uncertainty model shown in Table 3.

F. Problem Definition

To minimize the performance degradation of the coaxial rotor UAV, robust design optimization has been performed for two cases. In the first case, the optimization is performed to maximize the FM of the coaxial rotor. On the other hand, the available power $P_{\text{available}}$ is maximized in the second case, which dictates that the vertical climb and the maneuver in forward flight are enabled. The objective functions for each case are formulated by the weighted sum of both the performance and its deviation.

Case 1: Maximize *Figure of Merit* in hover

$$\begin{aligned}
&\text{Max.}\omega \cdot \text{FM} - (1-\omega)\cdot\sigma(\text{FM})\\
&\text{s.t. Thrust} = \text{GW}\\
&\quad \text{AI} - k\cdot\sigma(\text{AI}) \geq \text{AI}_{\text{baseline}}\\
&\quad W_{\text{blade}} + k\cdot\sigma(W_{\text{blade}}) \leq 1.3(W_{\text{blade}})_{\text{baseline}}\\
&\quad V_{\text{climb}} - k\cdot\sigma(V_{\text{climb}}) \geq (V_{\text{climb}})_{\text{baseline}}\\
&\quad P_{\text{available}} - k\cdot\sigma(P_{\text{available}}) \geq (P_{\text{available}})_{\text{baseline}}
\end{aligned}$$

Case 2: Maximize *available power* for vertical climb or forward flight

$$\begin{aligned}
&\text{Max.}\omega \cdot P_{\text{available}} - (1-\omega)\cdot\sigma(P_{\text{available}})\\
&\text{s.t. Thrust} = \text{GW}\\
&\quad \text{AI} - \text{k}\cdot\sigma(\text{AI}) \geq \text{AI}_{\text{baseline}}\\
&\quad \text{W}_{\text{blade}} + \text{k}\cdot\sigma(\text{W}_{\text{blade}}) \leq 1.3(\text{W}_{\text{blade}})_{\text{baseline}}\\
&\quad \text{V}_{\text{climb}} - \text{k}\cdot\sigma(\text{V}_{\text{climb}}) \geq (\text{V}_{\text{climb}})_{\text{baseline}}\\
&\quad \text{FM} - \text{k}\cdot\sigma(\text{FM}) \geq \text{FM}_{\text{baseline}}
\end{aligned}$$

where the subscript "baseline" represents the baseline coaxial rotor configuration given in Table 1. The terms GW and AI denote the gross weight and the autorotation index ($\text{AI} = I_R\Omega^2/2W$), respectively. W_{blade}, is the weight of blade and V_{climb} is the vertical climb rate. The standard deviation of F is represented by $\sigma(F)$. If $k = 0$ and $\omega = 1$, the formulation collapses to a DO problem that simply maximizes FM or $P_{\text{available}}$.

Since the optimization is carried out for hovering condition in the first and second cases, the required thrust must be equal to the gross weight of the coaxial rotor UAV. In addition, the AI of the designed rotor should be greater than the baseline value to guarantee safe landing. The W_{blade} is one of the crucial factors that affect the aerodynamic performance and the manufacturing cost. Hence, W_{blade} is constrained to have less than 1.3 times the baseline rotor weight. In other words, the W_{blade} should not exceed 1% of the gross take off weight (14 kg). Different from the first case, the second case deals with the objective function of $P_{\text{available}}$. Subsequently, an additional constraint condition is imposed such that FM should be greater than that of the baseline, which implies that the designed rotor generates sufficient power for hover.

The change in rotor geometry will result in a change in weight, which in turn affects the rotor performance such as FM and V_{climb}. Hence, the change in weight due to the variation of rotor geometry is taken into account. In addition, the conditions related to AI and W_{blade} are imposed to overcome a limitation of optimization design such as structural instability.

Table 3 Uncertainty models

Uncertainty factors		Mean	Deviation
Operating uncertainty	Damaged blade aera ($C_l = 0.6C_{l,\text{VR13}}$, $C_d = 3.0C_{d,\text{VR13}}$)	1.0 A	0.05 A
	weight (kg)	14.0	5.000×10^{-1}
Manufacturing uncertainty	Rotor diameter (M)	1.572	6.288×10^{-3}
	R_U/R_L	0.9	4.000×10^{-3}
	Twist (degree)	−11.0	1.200×10^{-1}
	Taper	2.0	4.000×10^{-2}

Table 4 Results of ANOVA (analysis of variance)

	Solidity (σ)	Figure of merits	C_T/σ	C_P/σ
R^2	0.9997	0.9985	0.9989	0.9993
RMSE	0.0095	0.0200	0.0170	0.0137

G. Construction of the Artificial Neural Network Models

To perform the efficient design optimization and accurately search for a robust region, an artificial neural network (ANN) model replaces the aerodynamic analysis. The ANN is a theory which mimics information processing of the human brain [30]. Similar to the human brain judging and perceiving phenomenon, the ANN can prove proper judgment or a value by clustering the information processing units called artificial neuron. Because the ANN characterizes to represent a nonlinearity, it can be incorporated to approximate a nonlinear function such as FM and C_P/σ.

Twenty-two experimental points for the shape of coaxial rotor blade are chosen via the D-optimal experimental design because design variables are four: the rotor diameter, the differential rotor radii (R_U/R_L), the taper, and the twist angle. Also, collective pitch angles of 3, 5, 7 and 9 deg are considered for the rotor trim. Therefore, a total of 88 experimental points are used to construct the ANN model. The ranges of design variables are summarized in Table 2. The aerodynamic analyses using the source-doublet panel method with a time-marching free wake model are performed for obtaining the FM, C_T/σ, and C_P/σ. The ANN models, which are composed of an input layer with five neurons (four design variables and one collective pitch angle), a hidden layer with eight neurons, and an output layer with four neurons (solidity, FM, C_T/σ, C_P/σ), are constructed. Note that the 88 experimental data points are used for model learning. The coefficient of determination R^2 and the root mean squared error (RMSE) are evaluated to validate the generation of alternative models, as summarized in Table 4. Of the entire approximate models, the coefficients of determination are greater than 0.99 and the RMSE are smaller than 0.02, thus ensuring reliable prediction capability of the artificial neural network models. Furthermore, Fig. 9 verifies that the value predicted by the meta-models agrees with the actual one, therefore lying in the ideal line.

III. Results

In this study, a DO is performed for a coaxial rotor configuration together with the RDO. By the DO, it represents any design method based on the deterministic concept without the concept of robustness. The hover performance function is approximated using the ANN in the design space. An optimal solution is sought by invoking a sequential quadratic programming method of PIAnO [31].

A. Pareto Optimal Sets

To solve the multi-objective problem of RDO in this study, the weighting function method is adopted due to easy implementation and fast generation of Pareto front. Figure 10 shows the Pareto front obtained from RDO with respect to the varying weight ω of the objective function from 0 to 1, together with increasing sigma level k. The weight ω is increased with the interval of 0.01 and 101 optimizations are performed to obtain the Pareto front for the fixed sigma level k. The k value is chosen such that it allows performing RDO, which is up to $k = 1.5$ in case 1 and is up to $k = 0.5$ in case 2. The x-axis represents the performance indices (FM and $P_{\text{available}}$) as the objective functions, while the y-axis represents the deviations of performance.

As shown in previous schematics, the feasible region is altered in the design space along with the increment of k. Subsequently, it results in the performance reduction with increased performance deviation, which ends up with weak robustness. On the other hand, the FM reveals that the size of the Pareto front shrinks, whereas the $P_{\text{available}}$ has opposite characteristics along with the increment of k. In general, when the feasible region shrinks due to the k value, one expects to obtain a plot as in Fig. 10. However, when one adopts a second-order polynomial, the plot is similar to the Pareto front of the $P_{\text{available}}$ plot. If k remains constant, the Pareto fronts corresponding

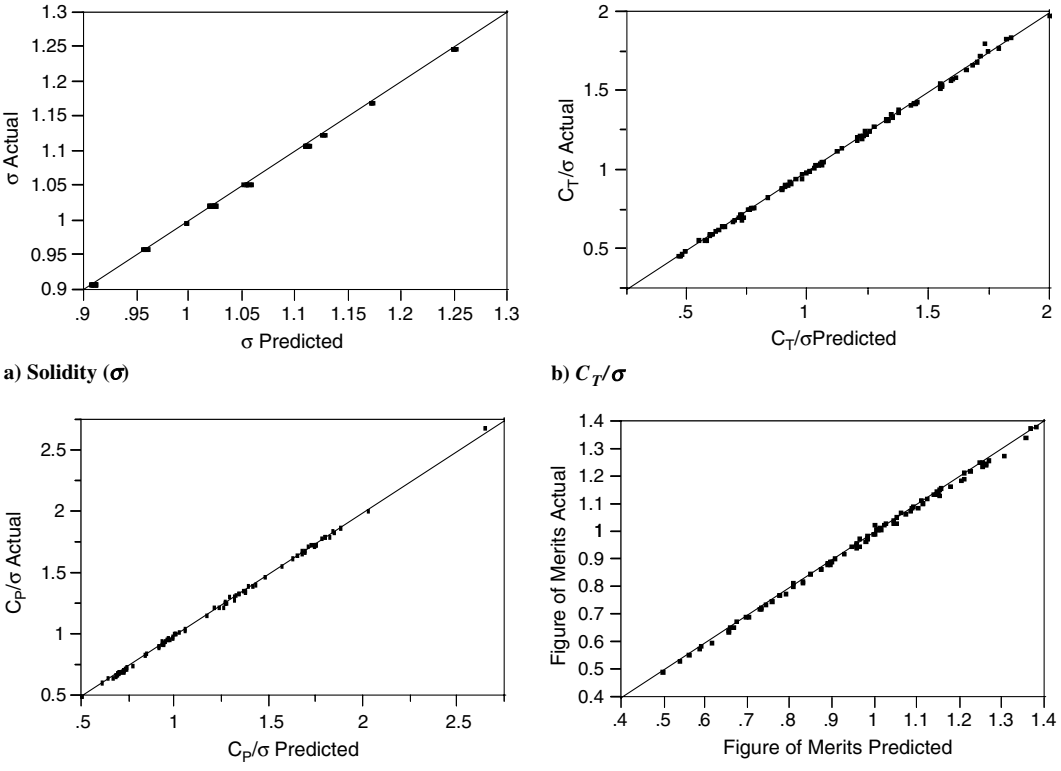

a) Solidity (σ) **b) C_T/σ**

c) C_P/σ **d) Figure of merits**

Fig. 9 Predicted values (x-axis) vs actual values (y-axis).

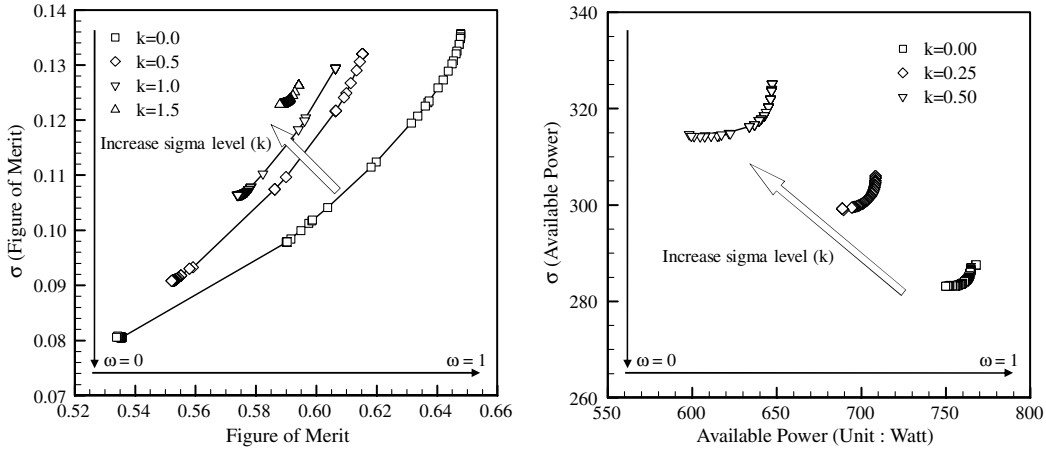

a) Figure of merit **b) Available power**

Fig. 10 Pareto optimal sets for FM and available power.

to FM and $P_{\text{available}}$ show the same characteristics. Because greater performance implies less robustness, or less performance implies more robustness, a tradeoff is necessary between them for the best results.

Figures 11 and 12 illustrate the information regarding the design variables related to the robustness (deviation) of the Pareto optima. In the case of maximizing FM (see Fig. 11), to assure the robustness of FM (or, to reduce the deviation of FM) the diameter and twist tend to decrease, while the R_U/R_L increases, yet the taper is almost constant (which reveals small effectiveness of taper for the robustness of FM). From these observations, the variables for the robustness of FM appear to contradict the physical intuition for improving FM. As a result, the design variables are determined by a tradeoff between the performance and the robustness. Next, for the robustness of the constraints, the increased k results in the bigger rotor diameter and the smaller taper. Nevertheless, the R_U/R_L and the twist turn out to have approximately the same values regardless of the value of k when taking into account the robustness ($k \neq 0$).

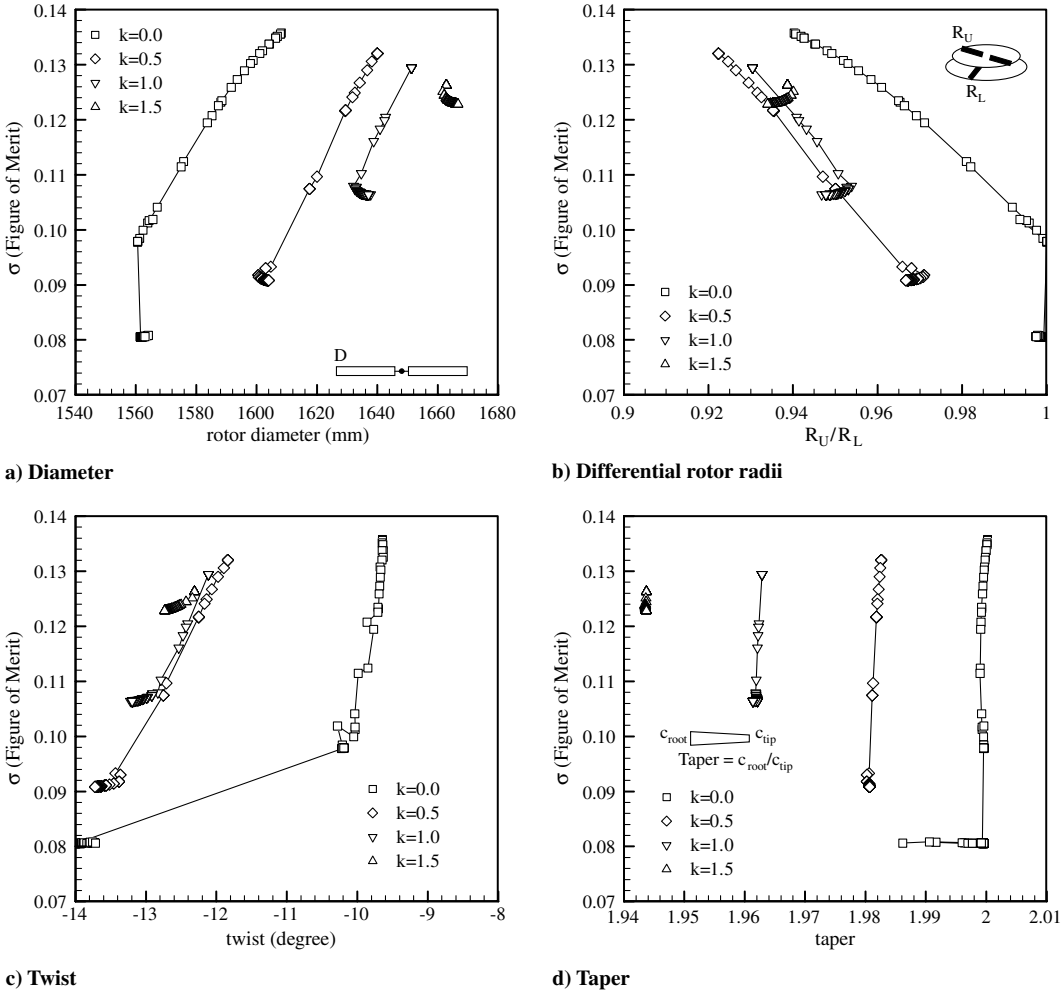

a) Diameter **b) Differential rotor radii**

c) Twist **d) Taper**

Fig. 11 Trend of design variables for robustness (maximum FM).

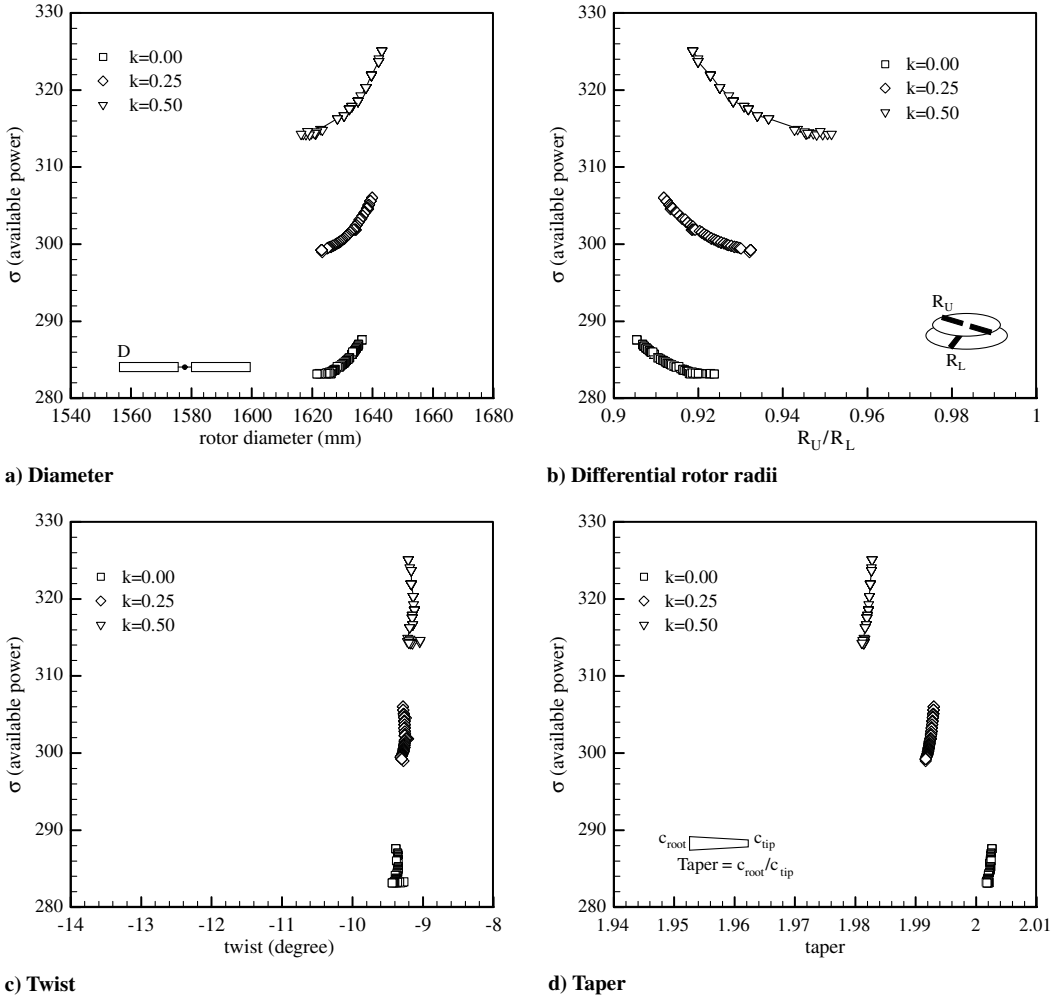

Fig. 12 Trend of design variables for robustness (maximum available power).

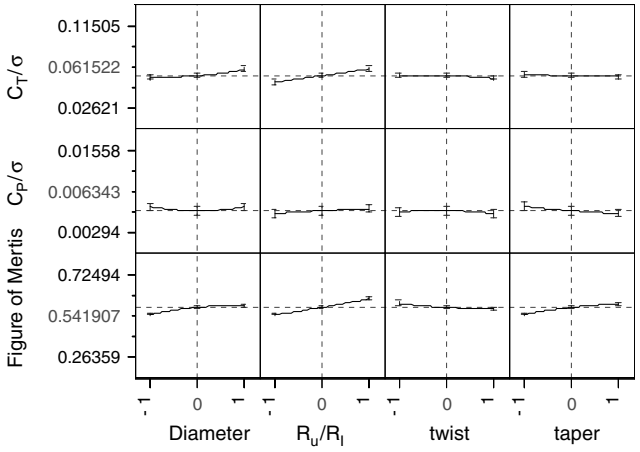

Fig. 13 Sensitivity chart of hover performance with respect to design variables.

In the case of $P_{available}$, as shown in Fig. 12, all plots show similar trends as the case of FM except the fact that the twist has little effect on the robustness. In contrast, three design variables (no taper variable) have almost same values with being little affected by *k*.

Figure 13 represents a sensitivity chart of design variables related to the hover performance when the thrust is fixed at 137.34 N by a collective pitch angle. The *x*-axis values −1 and 1 indicate the lower and upper bounds of each design variable which has been normalized from actual values. For instance, the twist varies from −14 to −8 deg, thus the lower bound −1 corresponds to −14 deg, and so on. As one can expect, the general trends shown in Fig. 13 agree with the physical intuition, namely, the FM is generally improved in conjunction with the increased rotor diameter, taper and twist angle.

In short, the trend of design variables (see Fig. 13) for improving FM and $P_{available}$ is opposite to the trend of each (see Figs. 11 and 12). Hence, it is imperative to find a tradeoff between the performance and the robustness. Unless this is the case, the higher performance indicates stronger robustness.

Table 5 Hover performance of the optimized coaxial rotors (maximum figure of merit)

	Baseline	Maximum figure of merit		
		Case 1-a	Case 1-b	Case 1-c
Figure of merit, deviation	0.5396 ($\sigma = 0.1378$)	**0.6478** ($\sigma = 0.1357$)	**0.5347** ($\sigma = 0.0806$)	**0.5879** ($\sigma = 0.1228$)
Thrust, N	137.34	137.30	137.34	137.31
Autorotation index	9.2863	9.2872	9.2891	9.8151
Weight of blade, kg	0.5520	0.7175	0.7172	0.7129
Climb rate, m/ min	87.37	311.38	100.86	286.68
Available power, W	200.00	712.75	230.87	656.22

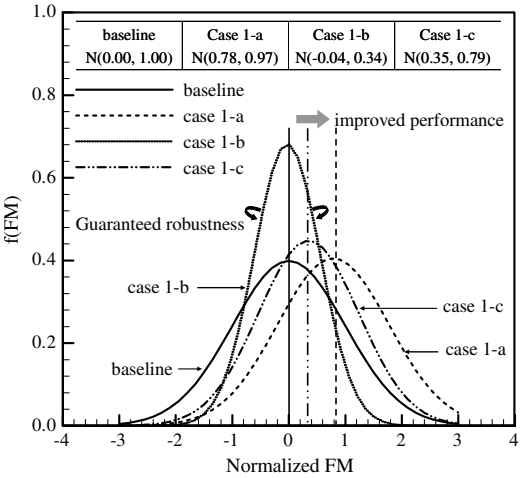

Fig. 14 Probability density function of FM.

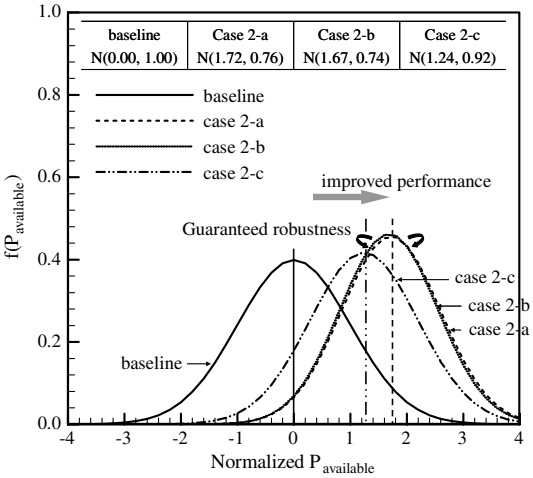

Fig. 15 Probability density function of available power.

B. Conventional Design Optimization vs Robust Design Optimization

Among the Pareto optimal points in Fig. 10, we choose three optima that have the following characteristic:

1) Case a: the case when the performance chosen for the objective function is maximally improved ($k = 0, \omega = 1$).

2) Case b: the case when the robustness for the objective function is maximally ensured ($k = 0, \omega = 0$).

3) Case c: the case when the robustness for the objective function and the constraints is ensured ($k \neq 0, \omega = 0$).

Case a represents the results of the DO, while cases b and care the results of the RDO where the minimum deviation of the objective function is found. Specifically, case b represents when the robustness of the objective function is solely dealt with by setting the k all to zeroes in the constraints. For case c, k is randomly chosen subject to the constraints. We investigate and compare the above three cases with respect to the maximizing FM and the maximizing $P_{\text{available}}$.

1. *Objective Functions*

Table 5 shows the optimized performance of the coaxial rotor UAV that maximizes FM at given constant thrust. The objective function of FM is represented in a bold typeface, and the active constraints are in an italic typeface. The sizes of the uncertainty models for the damaged area and the weight are chosen to be 5% damaged area and 0.5 kg weight increase, hence resulting in the deviation of FM. The size of uncertainty is chosen by half of the design requirements since the uncertainty varies within $\pm\sigma$ from a nominal value. In Table 5, means of FM are the performance of the undamaged blade, and deviation of FM means the degradation of FM when ballistic damage and the variation of weight are occurred. That is, if the rotor blade of Case 1-c is damaged, the FM will be reduced from 0.5879 to 0.3423 ($=0.5879 - 0.1228 * 2$), with the probability of 95%. In the case of the baseline, the FM of the damaged blade is 0.2640 ($=0.5396 - 0.1378 * 2$) and the degradation of FM shows 51%. However, through the robust design optimization process, the performance degradation of Case 1-c is reduced by 42% which is less than 51% of the baseline.

Figure 14 shows the probability density function of FM corresponding to the case in Table 5, where we assumed that the performance of the baseline corresponds to a normal distribution with zero-mean and variance 1, or $N(0, 1)$.

The FM for all optimized cases show the improvement by maximally 20% (case 1-a) over the baseline design. In the case 1-b when we only focus on reducing the deviation, the performance is improved by 1%, more or less, which dictates negligible improvement. In addition, the performance in case 1-c is improved by 9%

Table 6 Hover performance of the optimized coaxial rotors (maximum available power)

	Baseline	Maximum available power		
		Case 2-a	Case 2-b	Case 2-c
Figure of merit	0.5396	0.6331	0.6438	0.6135
Thrust, N	137.34	137.27	137.30	137.33
Autorotation index	9.2863	9.2874	9.2881	9.4561
Weight of blade, kg	0.5520	0.7175	0.7176	0.7161
Climb rate, m/ min	87.37	333.14	327.56	265.36
Available power, W (deviation, $\times 10^2$)	200.00 ($\sigma = 3.2836$)	**764.86** ($\boldsymbol{\sigma = 2.8698}$)	**749.78** ($\boldsymbol{\sigma = 2.8316}$)	**607.41** ($\boldsymbol{\sigma = 3.1419}$)

Table 7 Violation probability of constraints and the sigma level ($n\sigma$)

	Max. figure of merit			Max. available power		
	Case 1-a	Case 1-b	Case 1-c	Case 2-a	Case 2-b	Case 2-c
Figure of merit	——	——	——	25.3% (0.66σ)	23.0% (0.74σ)	30.0% (0.53σ)
Autorotation index	**49.9%** (**0.00$\boldsymbol{\sigma}$**)	**49.7%** (**0.01$\boldsymbol{\sigma}$**)	5.7% (1.58σ)	**49.9%** (**0.00$\boldsymbol{\sigma}$**)	**49.8%** (**0.01$\boldsymbol{\sigma}$**)	30.5% (0.51σ)
Weight of blade, kg	**48.6%** (**0.03$\boldsymbol{\sigma}$**)	**45.2%** (**0.12$\boldsymbol{\sigma}$**)	5.9% (1.56σ)	**49.0%** (**0.03$\boldsymbol{\sigma}$**)	**50.0%** (**0.00$\boldsymbol{\sigma}$**)	30.8% (0.50σ)
Climb rate, m/ min	3.8% (1.78σ)	**45.7%** (**0.11$\boldsymbol{\sigma}$**)	5.7% (1.58σ)	2.6% (1.94σ)	2.9% (1.89σ)	8.1% (1.40σ)
Available power, W	3.6% (1.80σ)	**45.7%** (**0.11$\boldsymbol{\sigma}$**)	5.5% (1.60σ)	——	——	——

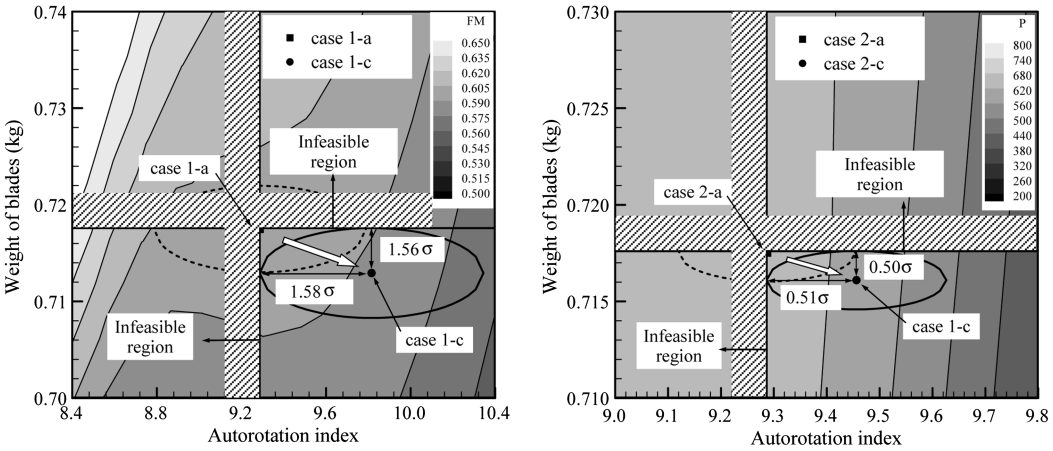

a) Maximum *figure of merit* **b) Maximum *available power***

Fig. 16 Active constraints and confidence intervals.

over the baseline design, which is at the same time 9% reduction from case 1-a. On the other hand, case 1-a shows a negligible deviation of FM over the baseline design, while cases 1-b and 1-c show the reduction of deviation of FM by 41% and 10%, respectively. As mentioned earlier, the reduction of the deviation means the increased robustness, hence allowing minimization of the performance degradation over uncertainty for successful mission accomplishments.

For the case of maximizing $P_{\text{available}}$ at constant thrust, Table 6 and Fig. 15 summarize the results in a similar manner in Table 5 and Fig. 14. The $P_{\text{available}}$ performance appears similar to the results as shown in Table 5 such that the performance decreases along the order of cases 2-a, 2-b, and 2-c. In contrast, the deviation shows different results such as $4 \sim 14\%$ reduction from the baseline design. However, the deviations in case 2-a (without considering the robustness) and case 2-b (that takes into account the robustness of the objective function) turn out to be 2% in each case. Thus, it can be told that no performance degradation of $P_{\text{available}}$ is observed. This is attributed to the fact that in a given design space, both the optimal point by the DO and the optimal point by the RDO are located at the same place. Meanwhile, the deviation in case 2-c is larger than that in case 2-a from the DO. As pointed out in the previous schematics, the increase of k induces a change of the feasible region in the design space to ensure the robustness of constraints, hence resulting in excluding certain regions that have good performance and robustness. As a result, even the RDO in case 2-c yields bigger deviations over that of the DO.

2. *Constraints*

Table 7 summarizes the probability of violated constraints and sigma level $n\sigma$, where active constraints are written in bold face. Both the DO (case 1-a, case 2-a) and the RDO (case 1-b and case 2-b) only for the robustness of the objective function ($k = 0$) have 50% of the probability of violation with respect to the constraints regarding AI and W_{blade}. The RDO taking into account the robustness of the objective function and constraints ($k \neq 0$); however, this ensures the confidence level of 1.5σ and 0.5σ, respectively.

The confidence levels of optimum point with respect to AI and W_{blade} constraints are shown in Fig. 16. The optimum point in case 1-a is located at the boundary of each constraints while the optimum in case 1-c is found to be relocated in the safe region, or within the feasible region. The confidence intervals corresponding to each optimum point are drawn by ellipses, which represent the regions where the performance variations are allowed. Thus, the AI in the case 1-c corresponds to the probability of achieving the target value by 5.7% upon the ballistic damage of 10% of the blade area.

As shown in the figures, each confidence interval does not overlap with the infeasible region but stays in the feasible region. Hence, it is possible to conclude that RDO ensures the robustness of constraints. This fact claims several meaningful results that the optimized coaxial rotor is likely to achieve a safe landing under emergency situation, as well as the reduction of the required power from decreasing the W_{blade}. In other words, the optimized coaxial rotor UAV designed by RDO is likely to meet the safety criterion, while accomplishing the missions successfully.

3. *Design Variables*

The geometric parameters of the optimized coaxial rotor configurations are shown in Table 8. The increase in the rotor diameter induces several disadvantages such as the overall dimension, cost, weight, and the torque limit of the gear box. The main concern is to determine the smallest rotor diameter which guarantees a safe landing. The reason why rotor diameter does not hit the upper bound is attributed by incorporating the AI. In addition, excessive taper may cause the low Reynolds number effect around the tip region, thus leading to structural instability. To prevent the blade from ending up with an overly slender tip, the W_{blade} constraint is imposed such that the taper ratio does not exceed 2, as given in Table 8. By employing the maximum taper ratio of 2, it could be possibly expected that the 5–6% decrease in the induced power by tapering the outer 50% of the blade span with a factor of 2 [25].

Andrew [32] and Leishman [3] discussed the possibility of improving coaxial rotor performance through the use of different sizes of the upper and the lower rotors. It follows from the analytical

Table 8 Geometry of the optimized coaxial rotors

		Rotor diameter, mm	R_U/R_L	Twist, deg	Taper	Solidity (σ)
Baseline		1572.00	1.00	0.00	1.00	0.0955
Maximum figure of merit	Case 1-a	1608.17	0.94	−9.64	2.00	0.0959
	Case 1-b	1562.27	1.00	−13.84	2.00	0.0963
	Case 1-c	1666.72	0.93	−12.74	1.94	0.0919
Maximum available power	Case 2-a	1635.33	0.91	−9.36	2.00	0.0957
	Case 2-b	1621.55	0.92	−9.44	2.00	0.0958
	Case 2-c	1619.09	0.95	−9.15	1.98	0.0948

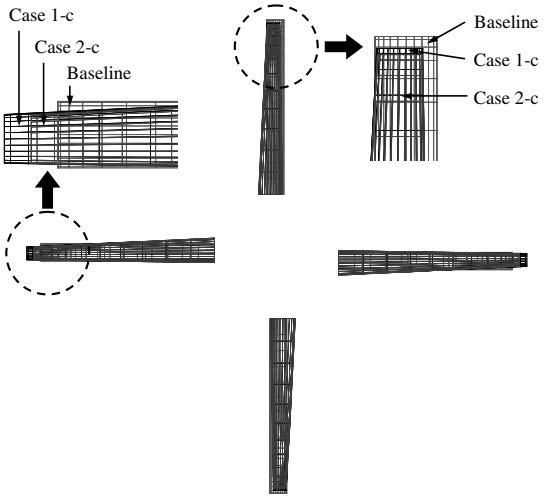

Fig. 17 Optimized coaxial rotor configurations (baseline, case 1-c and case 2-c).

model that decreasing the upper rotor radius by 8% could improve hover performance, which is due to the fact that the lower rotor disc takes undisturbed air over a larger portion instead of disturbed air downstream after the upper rotor disc. The results of R_U/R_L in Table 8 are consistent with the discussion given by Andrew [32] and Leishman [3].

To ensure the robustness of the objective function in the RDO as compared with the DO (case 1-a, case 2-a), the rotor diameter should be reduced (case 1-b, case 2-b). In contrast, the rotor diameter should be increased for the robustness of the AI constraint. (case 1-c, case 2-c) From this tradeoff relationship, case 1-c and case 2-c are ascertained to yield the proper diameter along with appropriate choice of the sigma level. Also, because the taper in the problem of maximizing FM or $P_{\text{available}}$ must be determined along with the variation of k value, which ends up with slight decrease to assure the robustness of the W_{blade} constraint. The results of R_U/R_L and twist are shown such that the design is done not to ensure the robustness but to improve the rotor performance. The coaxial rotors for UAV proposed from this research are case 1-c and case 2-c as shown in Fig. 17.

4. Summary

Figure 18 shows a six-axis radial graph presenting the performance of the optimized coaxial rotor. The graph compares the relative performances of each optimized coaxial rotor, which are normalized by the performance of DO (cases 1-a and 2-a). It can be verified from Fig. 18a that the results from RDO for robustness of the objective function (cases 1-b and 2-b) yield a significant decrease of the performance subject to the constraints. However, by introducing the sigma level to the constraints (cases 1-c and 2-c) the robustness of the objective function is ensured with little degradation of the other performance. Consequently, even though RDO finds results with low performance as opposed to DO, it has an advantage of not only ensuring the robustness of objective function but also minimizing the performance degradation due to constraints.

C. Off-Design Analysis

We perform the off-design analysis on the optimized coaxial rotor. Figure 19 shows the hover performance, which reveals the superior

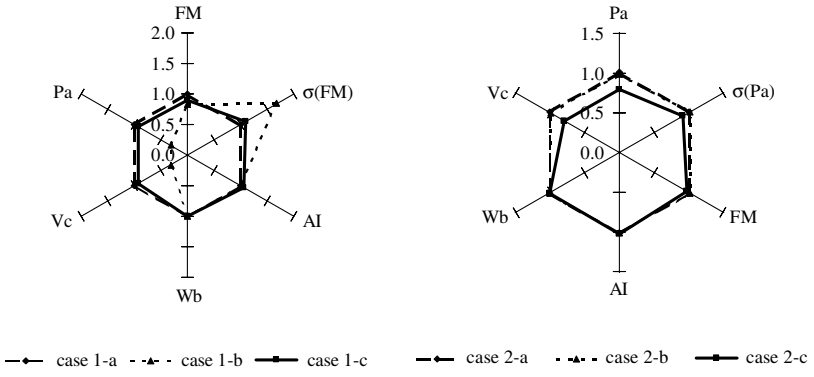

a) Maximum *figure of merit* **b) Maximum *available power***

Fig. 18 Performance indices of the optimized coaxial rotors.

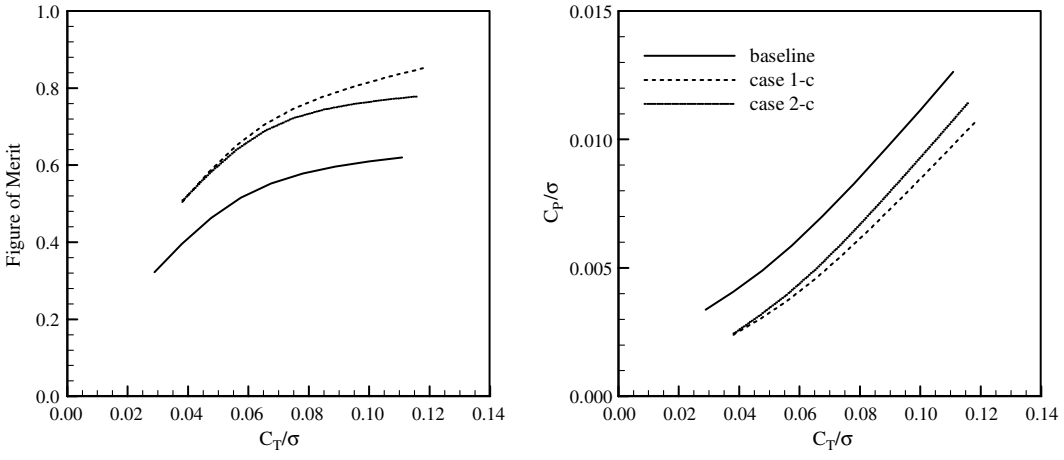

Fig. 19 Hover performance of optimized coaxial rotors.

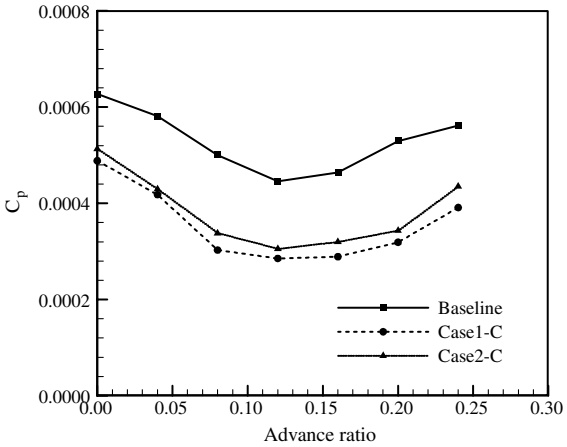

Fig. 20 Forward flight performance of optimized coaxial rotors.

performances of the RDO result (cases 1-c and 2-c) over the baseline design.

On the other hand, a coaxial rotor with a smaller advance ratio than 0.1 needs smaller required power over a single rotor with identical solidity due to the reduction of induced power. The coaxial rotor UAV in this study has the operation range of the advance ratio as small as less than 0.1. Subsequently, improved hover performance may result in the improvement of the forward flight performance as well. Hence, we analyze the forward flight of the designed coaxial rotor configurations, which are shown in Fig. 20 for C_P with respect to the forward speed. The results of RDO (cases 1-c and 2-c) also show improvement from the baseline design. Therefore, the RDO taking into account uncertainty is an appropriate approach for the design of coaxial rotor design.

IV. Conclusions

Robust design optimization for coaxial rotor is performed to maximize the performance and to minimize the performance degradation caused by uncertainties such as ballistic damage of rotor blade, weight variation due to mission change, and toleration of the geometry. Multi-objective functions consist of rotor performance and its deviation by incorporating four design variables of rotor diameter, differential rotor ratio, twist, and taper, which are to be optimized for robust rotor blade under uncertainties. From these results, the following statements can be concluded.

First of all, a coaxial rotor design is performed that satisfies the design requirements by employing either a DO or the RDO. By the conventional design, the probability to accomplish the missions in success under uncertainties such as ballistic damage or weight variation goes up as low as 50%, however, the probability can be improved by $70 \sim 95\%$ by employing the robust design method. Consequently, even with 10% blade damage and 1 kg of weight increase the optimized coaxial rotor UAV from RDO is most likely to accomplish missions in success. The optimized coaxial rotor is validated by the off-design analysis of hover and forward flight performances.

Second, the Pareto optimal set is obtained by modifying weights of the multi-objective function, and subsequently a tradeoff relationship between two optimization cases for figure of merit and available power is confirmed. The robustness is ensured by reduced performance deviation in conjunction with smaller rotor diameter and larger differential rotor radii, resulting in minimum performance degradation. Small twist ensures the robustness of figure of merit, yet is a contrary effect on available power. The taper has no effect on the robustness of figure of merit and available power. This tendency contradicts the anticipated tendency of design variables to improve performance.

Finally, the cases where the feasible region in the design space is altered in conjunction with the increase of the sigma level to ensure the robustness of constraints are encountered. This results in a modification of the region that contains not only good performance design but also strong robust design. In particular, in the case of the available power, the optimum point obtained from a conventional design matches with the robust optimum; thus, both the performance and the robustness are diminished when the sigma level changes.

Acknowledgments

This work was supported by the second stage of the Brain Korea 21 Project and the Analysis of Human Factor and Simultaneously Aerodynamic Performance Analysis for Rotorcraft Project of Korea Aerospace Research Institute.

References

[1] Leishman, J. G., and Ananthan, S., "Aerodynamic Optimization of a Coaxial Prop Rotor," *62nd Annual Forum and Technology Display of the American Helicopter Society*, AHS International, Alexandria, VA, May 2006.

[2] Byun, Y., Lee, J., Yee, K., Gu, T., Song, W., and Kang, B., "Re-Design of the Coaxial UAV's Platform for an Improvement in Performance," *Proceeding of the 2007 KSAS Fall Conference*, KSAS Paper 07-2204, 2007.

[3] Leishman, J. G., *Principles of Helicopter Aerodynamics*, 2nd ed., Cambridge University Press, Cambridge, 2006.

[4] Taguchi, G., *Taguchi on Robust Technology Development*, ASME Press, New York, 1993.

[5] DeLaurentis, D. A., and Mavris, D. N., "Uncertainty Modeling and Management in Multidisciplinary Analysis and Synthesis," AIAA Paper 2000-4222000.

[6] Du, X., and Chen, W., "Efficient Uncertainty Analysis Methods for Multidisciplinary Robust Design," *AIAA Journal*, Vol. 40, No. 3, 2002, pp. 545–552. doi:10.2514/2.1681

[7] Youn, B. D., Choi, K. K., and Park, Y. H., "Hybrid Analysis Method for Reliability-Based Design Optimization," *Journal of Mechanical Design*, Vol. 125, No. 2, 2003, pp. 221–232. doi:10.1115/1.1561042

[8] Putko, M. M., Newman, P. A., Taylor, A. C., III., and Green, L. L., "Approach for Uncertainty Propagation and Robust Design in CFD Using Sensitivity Derivatives," *Proceedings of the 15th AIAA Computational Fluid Dynamics Conference*, AIAA Paper 2001-2528, June 2001.

[9] Jun, S., Jeon, Y., Rho, J., Kim, J., Kim, J., and Lee, D., "Reliability-Based and Robust Design Optimization with Artificial Neural Network," *6th World Congresses of Structural and Multidisciplinary Optimization*, The International Society for Structural and Multidisciplinary Optimization, Daejon, Korea, May–June 2005.

[10] Murugan, S., Harursampath, D., and Ganguli, R., "Material Uncertainty Propagation in Helicopter Nonlinear Aeroelastic Response and Vibration Analysis," *AIAA Journal*, Vol. 46, No. 9, 2008, pp. 2332–2344. doi:10.2514/1.35941

[11] Murugan, S., Ganguli, R., and Harursampath, D., "Aeroelastic Response of Composite Helicopter Rotor with Random Material Properties," *Journal of Aircraft*, Vol. 45, No. 1, 2008, pp. 306–322. doi:10.2514/1.30180

[12] Leishman, J. G., "Aerodynamic Performance Considerations in the Design of a Coaxial Proprotor," *Journal of the American Helicopter Society*, Vol. 54, No. 1, Article No. 012005, 2009. doi:10.4050/JAHS.54.012005

[13] Leishman, J. G., and Ananthan, S., "An Optimum Coaxial Rotor System for Axial Flight," *Journal of the American Helicopter Society*, Vol. 53, No. 4, 2008, pp. 366–381. doi:10.4050/JAHS.53.366

[14] Wachspress, D. A., and Quackenbush, T. R., "Impact of Rotor Design on Coaxial Rotor Performance, Wake Geometry and Noise," *62nd Annual Forum and Technology Display of the American Helicopter Society*, AHS International, Alexandria, VA, May 2006.

[15] Lee, J., Yee, K., and Oh, S., "Parametric Study for Hovering Performance of a Coaxial Rotor UAV," *Journal of Aircraft*, Vol. 47, No. 5, 2010, pp. 1517–1530. doi:10.2514/1.46460

[16] Lee, J., Yee, K., and Oh, S., "Aerodynamic Characteristic Analysis of Multi-Rotors Using a Modified Free-Wake Method," *Transactions of the Japan Society for Aeronautical and Space Sciences*, Vol. 52, No. 177, 2009, pp. 168–179. doi:10.2322/tjsass.52.168

[17] Ganguli, R., "Survey of Recent Developments in Rotorcraft Design Optimization," *Journal of Aircraft*, Vol. 41, No. 3, 2004, pp. 493–510. doi:10.2514/1.58

[18] Celi, R., "Recent Applications of Design Optimization to Rotorcraft-A Survey," *Journal of Aircraft*, Vol. 36, No. 1, 1999, pp. 176–189. doi:10.2514/2.2424

[19] Bhadra, S., and Ganguli, R., "Aeroelastic Optimization of a Helicopter Rotor Using Orthogonal Array-Based Metamodels," *AIAA Journal*, Vol. 44, No. 9, 2006, pp. 1941–1951. doi:10.2514/1.11776

[20] Murugan, S., and Ganguli, R., "Aeroelastic Stability Enhancement and Vibration Suppression in a Composite Helicopter Rotor," *Journal of Aircraft*, Vol. 42, No. 4, 2005, pp. 1013–1024. doi:10.2514/1.5652

[21] Viswamurthy, S. R., and Ganguli, R., "Optimal Placement of Piezoelectric Actuated Trailing-Edge Flaps for Helicopter Vibration Control," *Journal of Aircraft*, Vol. 46, No. 1, 2009, pp. 244–253. doi:10.2514/1.38199

[22] Jun, S., Jeon, Y., Kim, J., and Lee, D., "Application of the Robust and Reliability-Based Design Optimization to the Aircraft Wing Design," *Journal of the Korea Society for Aeronautical and Space Sciences*, Vol. 34, No. 8, 2006, pp. 24–32.

[23] Papoulis, A., and Pillai, S. U., *Probability, Random Variables and Stochastic Processes*, 4th ed., McGraw–Hill, New York, 2002.

[24] Lee, B., Seo, J., Byun, Y., Kim, J., Yee, K., and Kang, B., "Development and Verification of Small-Scale Rotor Hover Performance Test-Stand," *Journal of the Korea Society for Aeronautical and Space Sciences*, Vol. 37, No. 10, 2009, pp. 975–983.

[25] Seo, J., Lee, B., Kang, B., Oh, S., and Yee, K., "Experimental Study on the Small-Scale Rotor Hover Performance in Partial Ground Conditions," *Journal of the Korea Society for Aeronautical and Space Sciences*, Vol. 38, No. 1, 2010, pp. 12–21.

[26] Nagashima, T., and Nakanishi, K., "Optimum Performance and Wake Geometry of Coaxial Rotor in Hover," *Proceedings of the 7th European Rotorcraft and Powered Lift Forum*, Royal Aeronautical Society Paper No. 41, 1981.

[27] Leishman, J. G., "Experimental Investigation into the Aerodynamic Characteristics of Helicopter Rotor Airfoils with Ballistic Damage," United States Army Research Laboratory Rept. ARL-CR-295, 1996.

[28] Potapczuk, M. G., and Reinmann, J. J., "Icing Simulation: A Survey of Computer Models and Experimental Facilities," AGARD CP-496, 1991, pp. 5.1–5.27.

[29] Kim, H., Bragg, B. M., "Effects of Leading-Edge Ice Accretion Geometry on Airfoil Aerodynamics," AIAA Paper 99-3150, 1999.

[30] Freeman, J. A., and Skapura, D. M., *Neural Networks Algorithm, Applications, and Programming Techniques*, Addison Wesley Longman, Reading, MA, 1992, Chap. 3.

[31] PIAnO (Process Integration, Automation and Optimization) User's Manual, Version 2.4, FRAMAX, Inc., Dec. 2008.

[32] Andrew, M. J., "Coaxial Rotor Aerodynamics in Hover," *Vertica*, Vol. 5, No. 2, 1981, pp. 163–172.